A Novel Finite-Element Method for Nonreciprocal Magneto-Photonic Crystal Waveguides

Naoya Kono and Yasuhide Tsuji, *Member, IEEE*

***Abstract*—A new formulation of the finite-element method to analyze nonreciprocal waveguides in magneto-photonic crystals (MPCs) is proposed. Accurate solutions of light propagations for two different directions are obtained by the asymmetrical input condition. As numerical examples, the performance of a waveguide-type optical isolator in MPCs designed by the eigenmode analyses is confirmed by using this method. Subsequently, an effective way to enhance the nonreciprocity of the optical isolator is shown.**

***Index Terms*—Finite-element method (FEM), magnetooptic (MO) effect, nonreciprocal optical circuit device, perfectly matched layer (PML), photonic crystals (PCs).**

I. Introduction

THE SUBJECT of fabrication and investigation of photonic crystals (PCs) [1] has been actively pursued with the advance of nanofabrication technologies. PCs potentially have a variety of abilities, such as the facilitation of control of light propagation and localization and the suppression of spontaneous emission, due to their optical properties. Recently, new phenomena related to various applications, such as the tunability of PCs [2], [3] and optical multirefringence [4], have been exploited in PCs.

Even wider applications, such as the Faraday effect enhancement at a designed wavelength, can be realized in PCs using magnetooptic (MO) media, known as magneto-photonic crystals (MPCs) [5], [6]. The experimental verification and linear optical response of one-dimensional MPCs have been reported [7], and the application developments toward optical circuit devices, such as the mode converter [8] and the optical isolator [9], have also been started. However, these devices are based on the bulk crystals and, from the point of view of integration, the investigation of waveguide-type devices is indispensable.

In order to estimate the propagating characteristics of MO waveguides, a variety of analysis methods has been developed. For example, the finite-element method (FEM) [10] and finite-difference method [11] can be applied to z-independent waveguides. In addition, z-dependent, but reflectionless, structures have been analyzed by using the beam propagation method [12]. However, all of these methods cannot be applied to MPC waveguides, which have z-dependent periodicity and yield reflection. Therefore, the authors developed a novel numerical method, based on FEM, for MPC waveguides.

Manuscript received September 8, 2003; revised March 29, 2004.

The authors are with Division of Electronics and Information Engineering, Hokkaido University, Sapporo 060-8628, Japan.

Digital Object Identifier 10.1109/JLT.2004.831101

FEM is a powerful analysis method and can be applied to various optical waveguide discontinuity problems. In earlier FEM analyses, a mode expansion technique, which consumes much computational time, was required on the input and output waveguides, when FEM was applied to a finite region with discontinuities. Recently, a new FEM that does not require the mode expansion technique and is easily applied to photonic crystal waveguides has been proposed [13]. However, this FEM assumes the symmetrical input condition at the incidence planes and therefore cannot be directly applied to nonreciprocal waveguides. In order to treat nonreciprocal waveguides, the above FEM is reformulated, without the mode expansion technique, to the form that allows us to use asymmetrical input condition.

Subsequently, this method is applied to the optical isolators using MPC waveguides. The trials to construct the optical circuits utilizing PCs are currently in vogue, but the reflections at each constituent device are relatively large. Thus, the optical isolators will be an important optical device in order to insert such PC lightwave circuits into optical network systems in the future. This paper describes the design of a waveguide-type optical isolator in MPCs, by the guided mode analyses, and confirms its operation as an optical isolator by using the present method. Moreover, an effective way to enhance the nonreciprocity of this optical isolator is discussed.

II. FEM Formulation for Nonreciprocal Periodic Optical Waveguide Analysis

This section shows an FEM formulation for analysis of nonreciprocal periodic optical waveguides such as MPC waveguides. Although an FEM without the need of a mode expansion technique has been presented to analyze PC waveguides, this FEM assumes that symmetrical inputs are used on both sides of the incidence planes to satisfy the continuity condition of the electric and magnetic fields. Here, we use an asymmetrical input condition to treat nonreciprocal waveguides.

A. Basic Equation

We consider two-dimensional MPC waveguides as shown in Fig. 1, where the computational window is in the yz plane and there is no variation along the x direction ($\partial/\partial x = 0$). The relative permittivity and permeability tensors are

$$[\varepsilon] = \begin{bmatrix} \varepsilon_{xx} & 0 & 0 \\ 0 & \varepsilon_{yy} & \varepsilon_{yz} \\ 0 & \varepsilon_{zy} & \varepsilon_{zz} \end{bmatrix} \tag{1}$$

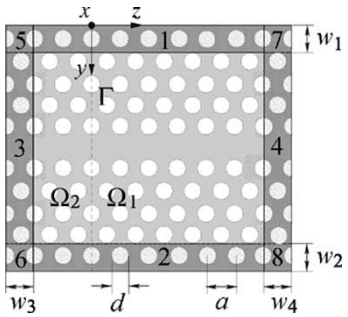

Fig. 1. MPC waveguide surrounded by PML.

TABLE I
PML PARAMETERS

PML parameter	PML region 1	2	3	4	5	6	7	8
s_y	s_1	s_2	1	1	s_1	s_2	s_1	s_2
s_z	1	1	s_3	s_4	s_3	s_3	s_4	s_4

$s_x = 1$ in all the PML regions.

$$[\mu] = \begin{bmatrix} \mu_{xx} & 0 & 0 \\ 0 & \mu_{yy} & 0 \\ 0 & 0 & \mu_{zz} \end{bmatrix} \tag{2}$$

where the propagation direction is the z direction and the direction of magnetization is the x direction. Surrounding the analysis region Ω by the anisotropic perfectly matched layer (PML) [14], [15], we can express the permittivity and permeability tensors as

$$[\varepsilon]_{\rm pml} = \begin{bmatrix} \tilde{\varepsilon}_{xx} & 0 & 0 \\ 0 & \tilde{\varepsilon}_{yy} & \tilde{\varepsilon}_{yz} \\ 0 & \tilde{\varepsilon}_{zy} & \tilde{\varepsilon}_{zz} \end{bmatrix} \tag{3}$$

$$\tilde{\varepsilon}_{xx} = \frac{s_y s_z}{s_x}\varepsilon_{xx}, \quad \tilde{\varepsilon}_{yy} = \frac{s_x s_z}{s_y}\varepsilon_{yy}, \quad \tilde{\varepsilon}_{zz} = \frac{s_x s_y}{s_z}\varepsilon_{zz}$$
$$\tilde{\varepsilon}_{yz} = s_x\varepsilon_{yz}, \quad \tilde{\varepsilon}_{zy} = s_x\varepsilon_{zy} \tag{4}$$

$$[\mu]_{\rm pml} = \begin{bmatrix} \tilde{\mu}_{xx} & 0 & 0 \\ 0 & \tilde{\mu}_{yy} & 0 \\ 0 & 0 & \tilde{\mu}_{zz} \end{bmatrix} \tag{5}$$

$$\tilde{\mu}_{xx} = \frac{s_y s_z}{s_x}\mu_{xx}, \quad \tilde{\mu}_{yy} = \frac{s_x s_z}{s_y}\mu_{yy}, \quad \tilde{\mu}_{zz} = \frac{s_x s_y}{s_z}\mu_{zz} \tag{6}$$

where the PML parameter s_i $(i = x, y, z)$ is summarized in Table I. The value of $s_k (k = 1, 2, 3, 4)$ in Table I is taken as

$$s_k = 1 - j\left(\frac{\rho}{w_k}\right)^2 \tan\delta_k \tag{7}$$

where ρ is the distance from the beginning of PML (PML surface), and δ_k is the loss angle at the end of PML ($\rho = w_k$). In the analysis region except for the PML region, we set $s_x = s_y = s_z = 1$.

In this case, Maxwell's equations are expressed as

$$\nabla \times \boldsymbol{H} = j\omega\varepsilon_0[\varepsilon]_{\rm pml}\boldsymbol{E} \tag{8}$$
$$\nabla \times \boldsymbol{E} = -j\omega\mu_0[\mu]_{\rm pml}\boldsymbol{H} \tag{9}$$

Considering $\partial/\partial x = 0$, from (8) and (9), we can obtain

$$\frac{\partial H_z}{\partial y} - \frac{\partial H_y}{\partial z} = j\omega\varepsilon_0\tilde{\varepsilon}_{xx}E_x \tag{10}$$
$$\frac{\partial H_x}{\partial z} = j\omega\varepsilon_0\tilde{\varepsilon}_{yy}E_y + j\omega\varepsilon_0\tilde{\varepsilon}_{yz}E_z \tag{11}$$
$$-\frac{\partial H_x}{\partial y} = j\omega\varepsilon_0\tilde{\varepsilon}_{zz}E_z + j\omega\varepsilon_0\tilde{\varepsilon}_{zy}E_y \tag{12}$$
$$\frac{\partial E_z}{\partial y} - \frac{\partial E_y}{\partial z} = -j\omega\mu_0\tilde{\mu}_{xx}H_x \tag{13}$$
$$\frac{\partial E_x}{\partial z} = -j\omega\mu_0\tilde{\mu}_{yy}H_y \tag{14}$$
$$-\frac{\partial E_x}{\partial y} = -j\omega\mu_0\tilde{\mu}_{zz}H_z. \tag{15}$$

Here, we consider transverse magnetic (TM) modes with nonreciprocal propagation property. From (11), (12), and (15), E_y and E_z are expressed as

$$E_y = \frac{1}{j\omega\varepsilon_0\tilde{\sigma}}\left(\tilde{\varepsilon}_{zz}\frac{\partial H_x}{\partial z} + \tilde{\varepsilon}_{yz}\frac{\partial H_x}{\partial y}\right) \tag{16}$$
$$E_z = \frac{1}{j\omega\varepsilon_0\tilde{\sigma}}\left(-\tilde{\varepsilon}_{yy}\frac{\partial H_x}{\partial y} - \tilde{\varepsilon}_{zy}\frac{\partial H_x}{\partial z}\right) \tag{17}$$
$$\tilde{\sigma} = \tilde{\varepsilon}_{yy}\tilde{\varepsilon}_{zz} - \tilde{\varepsilon}_{yz}\tilde{\varepsilon}_{zy}. \tag{18}$$

Substituting (16) and (17) to (13), we obtain the basic equation

$$\frac{\partial}{\partial y}\left(\frac{\tilde{\varepsilon}_{yy}}{\tilde{\sigma}}\frac{\partial H_x}{\partial y}\right) + \frac{\partial}{\partial z}\left(\frac{\tilde{\varepsilon}_{zz}}{\tilde{\sigma}}\frac{\partial H_x}{\partial z}\right) + \frac{\partial}{\partial y}\left(\frac{\tilde{\varepsilon}_{zy}}{\tilde{\sigma}}\frac{\partial H_x}{\partial z}\right) + \frac{\partial}{\partial z}\left(\frac{\tilde{\varepsilon}_{yz}}{\tilde{\sigma}}\frac{\partial H_x}{\partial y}\right) + k_0^2\tilde{\mu}_{xx}H_x = 0 \tag{19}$$

where H_x is the x components of the magnetic field, and k_0 is the free-space wavenumber.

B. Eigenmode Analysis

Dividing the analysis region into quadratic triangular elements, we can approximate the x component of the magnetic field H_x within each element as

$$H_x = \{N\}^T\{H_x\}_e \tag{20}$$

where $\{N\}$ is the shape function vector for the quadratic triangular element, and $\{H_x\}_e$ is the nodal H_x vector for each element.

In order to find out the propagation characteristics of PC waveguides, first the eigenmode of the periodic waveguide is calculated. The FEM is applied to the region of one period along the z direction, and the periodic boundary condition is imposed on the left and right boundaries Γ_1, Γ_2, as shown in Fig. 2. In this case, the periodic boundary conditions are given as

$$H_x|_{\Gamma_2} = \exp(-j\beta a)H_x|_{\Gamma_1} \tag{21}$$

and

$$\left(\frac{\tilde{\varepsilon}_{zz}}{\tilde{\sigma}}\frac{\partial H_x}{\partial z} + \frac{\tilde{\varepsilon}_{yz}}{\tilde{\sigma}}\frac{\partial H_x}{\partial y}\right)\Bigg|_{\Gamma_2} = \exp(-j\beta a)\left(\frac{\tilde{\varepsilon}_{zz}}{\tilde{\sigma}}\frac{\partial H_x}{\partial z} + \frac{\tilde{\varepsilon}_{yz}}{\tilde{\sigma}}\frac{\partial H_x}{\partial y}\right)\Bigg|_{\Gamma_1} \tag{22}$$

where β is the propagation constant, and a is the lattice constant. Applying the Galerkin procedure to (19), integrating

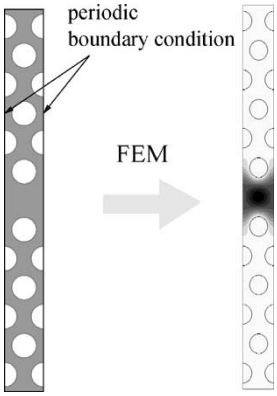

Fig. 2. Eigenmode analysis of PC waveguide.

by parts, considering (20) and assembling the contributions of all different elements, we can eliminate the boundary integral terms owing to the continuity conditions of electric and magnetic fields and obtain the generalized eigenvalue matrix equation (23)–(25), shown at the bottom of the page, where the components of vector $\{H_x\}$ are the values of H_x at all nodal points and $\sum_e$ extends over all elements.

C. Lightwave Propagation Analysis

In order to treat nonreciprocal waveguide discontinuity problems, we carry out the FEM analysis whose input condition is defined by the eigenmode obtained by the eigenmode analysis of the waveguides. We consider the incidence plane Γ, which is normal to the z axis, as shown in Fig. 1, and divide the whole region Ω into two subregions Ω_1 and Ω_2. By applying the Galerkin procedure to (19), integrating by parts, considering (20) and $H_x = 0$ at the outer boundary of PML, and assembling the contributions of all different elements except for the incidence plane Γ, we can eliminate the boundary integral terms due to the continuity conditions of electric and magnetic fields and obtain the following matrix equation for each subregion Ω_1, Ω_2:

$$[P_1]\{H_{x,1}\}=\{\Psi_1\} \tag{26}$$

$$[P_2]\{H_{x,2}\}=\{-\Psi_2\} \tag{27}$$

$$[P_i]=[K_i]-k_0^2[M_i] \tag{28}$$

$$\{\Psi_i\}=\sum_{e_i}{}' \int_{e_i} \{N\}_\Gamma \left(\frac{\tilde{\varepsilon}_{zz}}{\tilde{\sigma}}\frac{\partial H_{x,i}}{\partial z}+\frac{\tilde{\varepsilon}_{yz}}{\tilde{\sigma}}\frac{\partial H_{x,i}}{\partial y}\right)dy \tag{29}$$

where the subscript i denotes the values in the region $\Omega_i (i = 1, 2)$, $\{N\}_\Gamma$ is the shape function vector on the incidence plane, and $\sum'_{e_i}$ extends over the elements related to Γ_i.

Here, using the vector composed of the values of H_x at nodal points on the incidence plane Γ, $\{H_{x,i}\}_\Gamma$, and the vector related to the remaining nodes, $\{H_{x,i}\}_0$, we rewrite (26) and (27) as

$$\begin{bmatrix}[P_1]_{00} & [P_1]_{0\Gamma}\\ [P_1]_{\Gamma 0} & [P_1]_{\Gamma\Gamma}\end{bmatrix}\begin{bmatrix}\{H_{x,1}\}_0\\ \{H_{x,1}\}_\Gamma\end{bmatrix}=\begin{bmatrix}\{0\}\\ \{\Psi_1\}_\Gamma\end{bmatrix} \tag{30}$$

$$\begin{bmatrix}[P_2]_{00} & [P_2]_{0\Gamma}\\ [P_2]_{\Gamma 0} & [P_2]_{\Gamma\Gamma}\end{bmatrix}\begin{bmatrix}\{H_{x,2}\}_0\\ \{H_{x,2}\}_\Gamma\end{bmatrix}=\begin{bmatrix}\{0\}\\ -\{\Psi_2\}_\Gamma\end{bmatrix} \tag{31}$$

where $[P_i]_{00}$, $[P_i]_{0\Gamma}$, $[P_i]_{\Gamma 0}$, and $[P_i]_{\Gamma\Gamma}$ are the partial matrices of $[Pi]$.

Defining the incident field to Ω_i as $H_{x,\mathrm{in},i}$ and the scattering field as $H_{x,\mathrm{scat},i}$, we can express the field in Ω_i as

$$H_{x,i}=H_{x,\mathrm{in},i}+H_{x,\mathrm{scat},i} \tag{32}$$

and the continuity conditions of electric and magnetic fields on the incidence plane Γ are given by

$$\frac{\tilde{\varepsilon}_{zz}}{\tilde{\sigma}}\frac{\partial H_{x,\mathrm{scat},1}}{\partial z}+\frac{\tilde{\varepsilon}_{yz}}{\tilde{\sigma}}\frac{\partial H_{x,\mathrm{scat},1}}{\partial y} =\frac{\tilde{\varepsilon}_{zz}}{\tilde{\sigma}}\frac{\partial H_{x,\mathrm{scat},2}}{\partial z}+\frac{\tilde{\varepsilon}_{yz}}{\tilde{\sigma}}\frac{\partial H_{x,\mathrm{scat},2}}{\partial y} \tag{33}$$

$$H_{x,\mathrm{scat},1}=H_{x,\mathrm{scat},2}=H_{x,\mathrm{scat}}. \tag{34}$$

Then, combining (30) and (31) corresponding to the regions Ω_1 and Ω_2, we obtain the matrix equation

$$\begin{bmatrix}[P_1]_{00} & [0] & [P_1]_{0\Gamma}\\ [0] & [P_2]_{00} & [P_2]_{0\Gamma}\\ [P_1]_{\Gamma 0} & [P_2]_{\Gamma 0} & [P_1]_{\Gamma\Gamma}+[P_2]_{\Gamma\Gamma}\end{bmatrix}\begin{bmatrix}\{H_{x,1}\}_0\\ \{H_{x,2}\}_0\\ \{H_{x,\mathrm{scat}}\}_\Gamma\end{bmatrix} =\begin{bmatrix}-[P_1]_{0\Gamma}\{H_{x,\mathrm{in},1}\}_\Gamma\\ -[P_2]_{0\Gamma}\{H_{x,\mathrm{in},2}\}_\Gamma\\ \{\Psi_{\mathrm{in},1}\}_\Gamma-\{\Psi_{\mathrm{in},2}\}_\Gamma\\ -[P_1]_{\Gamma\Gamma}\{H_{x,\mathrm{in},1}\}_\Gamma-[P_2]_{\Gamma\Gamma}\{H_{x,\mathrm{in},2}\}_\Gamma\end{bmatrix} \tag{35}$$

where $\{\Psi_{\mathrm{in},i}\}_\Gamma$ is the vector excepting the scattering field from $\{\Psi_i\}_\Gamma$. In this formulation, the incident field $H_{x,\mathrm{in},i}$ for the $+z$ and $-z$ directions can be given individually.

Fig. 3 shows the magnetic field distribution in an MPC waveguide. The fundamental TM mode is inputted asymmetrically. We assume $d = 0.58a$, $\varepsilon_{xx} = 9.789$, $\varepsilon_{yy} = \varepsilon_{zz} = 10.0$, $\varepsilon_{yz} = -\varepsilon_{zy} = j0.368$ and the operating normalized frequency is $\omega a/(2\pi c)0.236$.

$$\left([K]-k_0^2[M]\right)\{H_x\}=\{0\} \tag{23}$$

$$[K]=\sum_e \int\int_e \left(\frac{\tilde{\varepsilon}_{yy}}{\tilde{\sigma}}\frac{\partial\{N\}}{\partial y}\frac{\partial\{N\}^T}{\partial y}+\frac{\tilde{\varepsilon}_{zz}}{\tilde{\sigma}}\frac{\partial\{N\}}{\partial z}\frac{\partial\{N\}^T}{\partial z}+\frac{\tilde{\varepsilon}_{zy}}{\tilde{\sigma}}\frac{\partial\{N\}}{\partial y}\frac{\partial\{N\}^T}{\partial z} +\frac{\tilde{\varepsilon}_{yz}}{\tilde{\sigma}}\frac{\partial\{N\}}{\partial z}\frac{\partial\{N\}^T}{\partial y}\right)dydz \tag{24}$$

$$[M]=\sum_e \int\int_e \tilde{\mu}_{xx}\{N\}\{N\}^T dydz \tag{25}$$

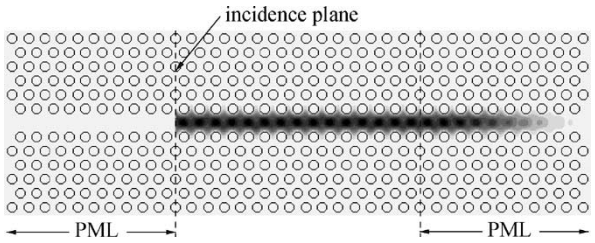

Fig. 3. Field distribution in a MPC waveguide inputted asymmetrically.

In the case of reciprocal waveguides, the relations $H_{x,\mathrm{in},1} = H_{x,\mathrm{in},2}$ and $\{\Psi_1\}_\Gamma = -\{\Psi_2\}_\Gamma = \{\Psi\}_\Gamma$ are satisfied in (35); then, (35) can be reduced to

$$\begin{bmatrix} [P]_{00} & [P]_{0\Gamma} \\ [P]_{\Gamma 0} & [P]_{\Gamma\Gamma} \end{bmatrix} \begin{bmatrix} \{H_x\}_0 \\ \{H_x\}_\Gamma \end{bmatrix} = \begin{bmatrix} \{0\} \\ 2\{\Psi\}_\Gamma \end{bmatrix} \tag{36}$$

$$[P]_{00} = \begin{bmatrix} [P_1]_{00} & [0] \\ [0] & [P_2]_{00} \end{bmatrix} \tag{37}$$

$$[P]_{0\Gamma} = \begin{bmatrix} [P_1]_{0\Gamma} \\ [P_2]_{0\Gamma} \end{bmatrix} \tag{38}$$

$$[P]_{\Gamma 0} = [[P_1]_{\Gamma 0} \quad [P_2]_{\Gamma 0}] \tag{39}$$

$$[P]_{\Gamma\Gamma} = [[P_1]_{\Gamma\Gamma} + [P_2]_{\Gamma\Gamma}]. \tag{40}$$

We can see that (36) is the same equation as the earlier FEM formulation, using the port truncation technique with PML boundary condition [13].

III. Numerical Examples

In order to confirm the accuracy of our approach, we apply it to analyses of optical isolators. The optical isolators considered here are based on coupled waveguides and designed by the eigenmode analyses of the composing waveguides. Lightwave propagation analyses, using the present method, are performed to confirm the performances of the optical isolators.

A. Design of the Optical Isolator Using MPC Waveguides

We consider nonreciprocal coupled MPC waveguides as shown in Fig. 4. The waveguides are created in MPCs by removing a row of air holes. Two waveguides, I and II, are parallel in the coupling region, and waveguide I is connected with the input waveguide. The compensation walls (CWs) [16] are introduced into the center of the waveguide II to induce nonreciprocity for TM modes, and the direction of magnetism is reversed at the CW. We design the waveguides to satisfy the phase-matching condition for only backward propagation. This design method is explained hereafter.

In our case, the diameter of the air holes is chosen to be $d = 0.58a$, where a is the lattice constant of the PC. The magnetization in each domain is directed along the x axis. Thus, the relative permittivity tensor of the magnetic materials is given as

$$[\varepsilon] = \begin{bmatrix} \varepsilon_0 + \beta m^2 & 0 & 0 \\ 0 & \varepsilon_0 & j\alpha m \\ 0 & -j\alpha m & \varepsilon_0 \end{bmatrix} \tag{41}$$

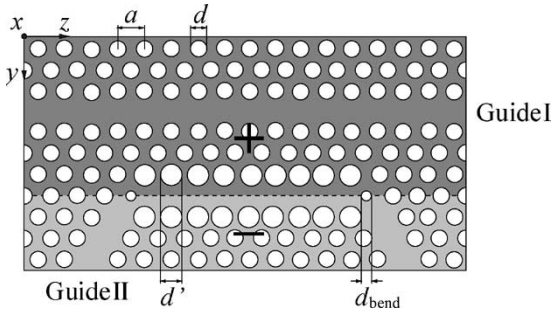

Fig. 4. Nonreciprocal coupled waveguide using MPCs.

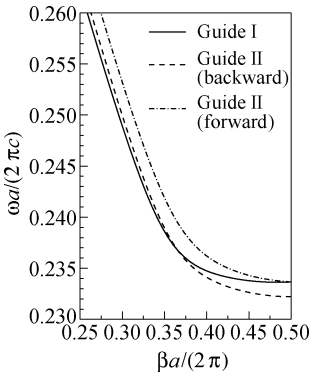

Fig. 5. Dispersion relations for each isolated waveguide.

where ε_0 is the permittivity of free space, α and β are the MO constants of the first and second order, respectively, $m = m_x/M_0$ and M_0 is the saturation magnetization of the medium. We numerically estimate the MO effects for Bi:YIG (Bi-substituted yttrium–iron–garnet) waveguides with $\alpha = -3.68 \times 10^{-1}$, $\beta = -2.11 \times 10^{-1}$, $\varepsilon = 10$, and for the light wavelength $\lambda = 1.15$ μm [8]. Now, we first assume the rate of magnetization of the medium is large as $m = 1.0$ to confirm the validity of our theory to nonreciprocal coupled waveguides. The relative permeability is given as $\mu_{xx} = \mu_{yy} = \mu_{zz} = 1.0$.

Fig. 5 shows the dispersion curves of each isolated waveguide composing the nonreciprocal coupler. Waveguide II has nonreciprocity, and so its propagation constants for forward and backward propagation are different. Here, we chose the diameter of the air holes adjoining to the waveguide II to be $d' = 0.60a$ so that the only backward-propagating light can satisfy the phase-matching condition with waveguide I. The phase-matching condition is satisfied at the intersection of the two dispersion curves of waveguides I and II. We study the frequencies close to the phase-matching condition as the operation frequency of the optical isolator.

Fig. 6 shows the dispersion curves of the coupled waveguide, in which waveguides I and II are regarded as one system. In this coupled waveguide, two nonreciprocal eigenmodes can propagate. Using the propagation constants β_{e} and β_{o} of these modes, the coupling length L is given as

$$L = \frac{\pi}{|\beta_{\mathrm{e}} - \beta_{\mathrm{o}}|}. \tag{42}$$

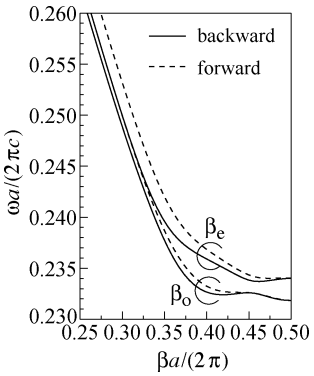

Fig. 6. Dispersion relations for coupled waveguide.

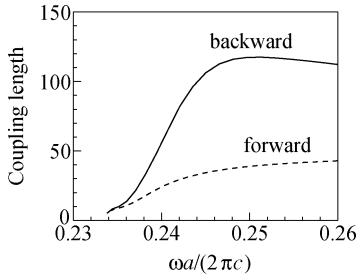

Fig. 7. Coupling length of the nonreciprocal coupler.

The coupling length calculated from (42) is shown in Fig. 7. The coupling length also has nonreciprocity, and if the coupling length for each propagation direction satisfies the following relation around the phase matching frequency:

$$2mL_{\text{forw}} = (2n-1)L_{\text{back}} \tag{43}$$

this coupled waveguide performs as an isolator at $z = (2n-1)L_{\text{back}}$. L_{forw} and L_{back} are the coupling lengths for forward and backward propagation, respectively, and m and n are the positive integers. In this case, the coupling length of backward propagation $L_{\text{back}} = 40a$ is twice as long as that of forward propagation $L_{\text{forw}} = 20a$, at the normalized frequency $\omega a/(2\pi c) = 0.238$. The operation wavelength is now assumed to be $\lambda = 1.15$ μm, and so the lattice constant is given as $a = 0.274$ μm.

Next, we have performed light propagation analyses at this frequency. At the edges of the coupling region, waveguide II is connected with bends to separate waveguides I and II, as shown in Fig. 4. If we used simple 60° bends, transmission loss of the bend would be 1.45 dB at the operation wavelength. To reduce the transmission loss, it is effective to add the optimum air holes at the bends to satisfy the impedance matching between the straight waveguides and the bends [17], [18]. In this example, the diameter of the additional air holes is chosen to be $d_{\text{bend}} = 0.42a$ so that the transmission loss of the bend is suppressed about 0.004 dB. The computational window size is set to be $65a$ for the propagation direction and $20a$ for the transverse direction. PML, with thickness $20a$, is placed on every computational window edge of the propagation direction, and the loss angle is assumed to be $\tan\delta = 0.05$.

Fig. 8 shows the field distributions in the designed optical isolator. For the forward propagation, the field inputted into waveguide I weakly couples to waveguide II and then couples back to the original waveguide I, while, for the backward propagation, it strongly couples to waveguide II once and then the optical power leaves the coupling region at the bend. Here, the reason for the weak coupling for the forward-traveling wave is the mismatch of the propagation constants between waveguides I and II, as shown in Fig. 5. Therefore, this device performs as an isolator. Our calculations also show that the isolation is 26.9 dB.

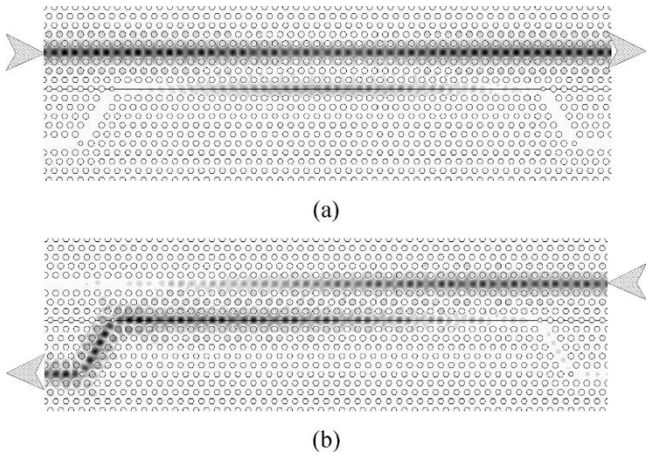

Fig. 8. Magnetic field distribution in the optical isolator (a) forward propagation and (b) backward propagation.

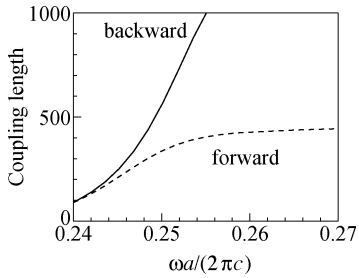

Fig. 9. Coupling length of the nonreciprocal coupler.

B. Nonreciprocity Enhanced MPC Waveguide Isolators

Even if the MO effect of the material itself is small, similar operation as shown in the previous section is possible, but the device length of the isolator increases due to the small nonreciprocity. Fig. 9 shows the calculated coupling length in the case of $m = 0.1$ in (41). The size of the lower side air holes is modified to satisfy the phase-matching condition for backward propagation. In this case, the coupling length of backward propagation $L_{\text{back}} = 740a$ is twice as long as that of forward propagation $L_{\text{forw}} = 370a$ at the normalized frequency $\omega a/(2\pi c) = 0.252$, and thus the device length of only the coupling part is given as $740a$. At the wavelength $\lambda = 1.15$ μm, the lattice constant is given as $a = 0.290\mu$m, and then the device length is approximately 214 μm.

For enhancing the nonreciprocity and reducing such device length, increasing confinement of fields in nonreciprocal waveguides is effective [19]. In MPC waveguides, the field locality can be enhanced by narrowing the width of the waveguides or enlarging the diameter of the air holes. Here, we consider the structure shown in Fig. 10, in which the diameter of the air holes ad-

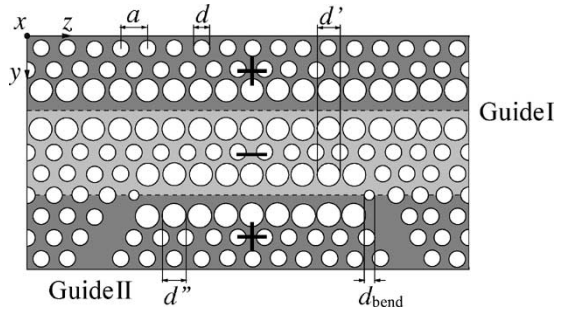

Fig. 10. Nonreciprocity enhanced MPC waveguide coupler.

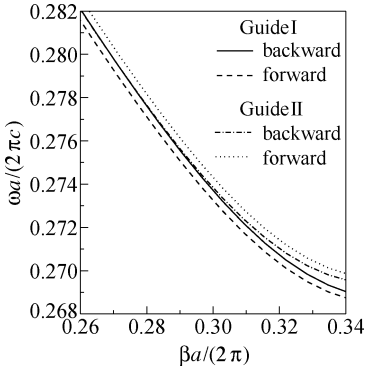

Fig. 11. Dispersion relations for each isolated waveguide of nonreciprocity enhanced MPC waveguide coupler.

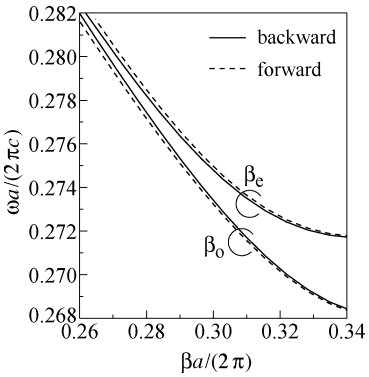

Fig. 12. Dispersion relations for nonreciprocity enhanced MPC waveguide coupler.

jacent to the waveguides is enlarged and CWs are introduced on the centers of the both waveguides. The diameter of the air holes on the both sides of waveguide I, the upper side of the waveguide II is set to be $d' = 0.90a$, and the diameter of the lower side air holes of waveguide II is changed to be $d'' = 0.91a$ to satisfy the phase-matching condition for backward propagation.

Fig. 11 shows the dispersion curves of each waveguide constituting the nonreciprocal coupler. In this case, both waveguides I and II have nonreciprocity, but the phase-matching condition is satisfied only for the backward propagation, the same as the previous section.

Fig. 12 shows the dispersion curves for the coupled waveguide in which waveguides I and II are regarded as one system. The coupling length, which can be estimated from (42), is then

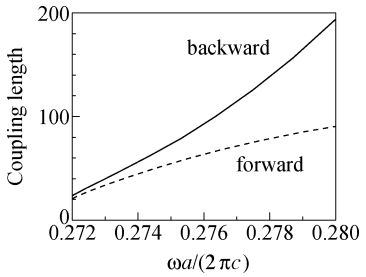

Fig. 13. Coupling length of the nonreciprocity enhanced MPC waveguide coupler.

shown in Fig. 13. In this case, the coupling length of backward propagation $L_{\rm back} = 173a$ is twice as long as that of forward propagation $L_{\rm forw} = 86.5a$ at the normalized frequency $\omega a/(2\pi c) = 0.279$, and thus this nonreciprocal coupler performs as an optical isolator when a length of the coupling region is chosen as $173a$. At the wavelength $\lambda = 1.15$ μm, the lattice constant is given as $a = 0.321$ μm, and the coupling region length then becomes 55.5 μm. Thus, the coupling region length is reduced by one fourth compared with that of the previous structure, i.e., 214 μm.

Finally, we have performed light propagation analyses at the operation frequency. Each side of the coupling region of waveguide II is connected with the low-loss bend, as shown in Fig. 10. The diameter of the additional air holes is set to be $d_{\rm bend} = 0.38a$. The computational window size is $196a$ for the propagation direction and $19a$ for the transverse direction. PML, with thickness $20a$, is placed on every window edge of the propagation direction, and the loss angle is assumed to be $\tan\delta = 0.05$. The field distributions are obtained similar to those in Fig. 8, and the isolation degree is 27.1 dB.

IV. Conclusion

A novel FEM was developed for the analysis of nonreciprocal MPC waveguides. In this approach, the asymmetrical input is possible. We designed optical isolators using MPC waveguides and confirmed the actual device operations as isolators by using the newly formulated FEM. These isolators are based on nonreciprocal coupled waveguides which satisfy the phase-matching condition for only one propagating direction. Using this design method, an optical isolator can be constituted from only one coupling length of the coupler. It was also shown that the nonreciprocity of the optical isolators can be enhanced by enlarging diameters of the air holes adjacent to MPC waveguides.

Acknowledgment

The authors would like to thank Prof. M. Koshiba of Hokkaido University, Sapporo, Japan, for his important comments and consideration.

References

[1] J. D. Joannopoulos, P. R. Villeneuve, and S. Fan, "Photonic crystals: putting a new twist on light," *Nature*, vol. 386, pp. 143–149, Mar. 1997.
[2] C. S. Kee, J. E. Kim, and H. Y. Park, "Heliconic band structure of one-dimensional periodic metallic composites," *Phys. Rev. E*, vol. 57, pp. 2327–2331, Feb. 1998.

[3] M. Scalora, J. P. Dowling, C. M. Bowden, and M. J. Bloemer, "Optical limiting and switching of ultrashort pulses in nonlinear photonic band gap materials," *Phys. Rev. Lett.*, vol. 73, pp. 1368–1371, Sept. 1994.
[4] M. C. Netti, A. Harris, J. J. Baumberg, D. M. Whittaker, M. B. D. Charlton, M. E. Zoorob, and G. J. Parker, "Optical trirefringence in photonic crystal waveguides," *Phys. Rev. Lett.*, vol. 86, pp. 1526–1529, Feb. 2001.
[5] E. Takeda, N. Todoroki, Y. Kitamoto, M. Abe, M. Inoue, T. Fujii, and K. Arai, "Faraday effect enhancement in Co-ferrite layer incorporated into one-dimensional photonic crystal working as a Fabry–Pérot resonator," *J. Appl. Phys.*, vol. 87, pp. 6782–6784, May 2000.
[6] M. Tanaka, H. Shimizu, and M. Miyamura, "Enhancement of magneto-optical effect in a GaAs:MnAs hybrid nanostructure sandwiched by GaAs/AlAs distributed Bragg reflectors: Epitaxial semiconductor-based magneto-photonic crystal," *J. Crystal Growth*, vol. 227/228, pp. 839–846, 2001.
[7] M. Inoue, K. I. Arai, T. Fujii, and M. Abe, "One-dimensional magnetophotonic crystals," *J. Appl. Phys.*, vol. 85, pp. 5768–5770, 1999.
[8] S. A. Nikitov and P. Tailhades, "Optical modes conversion in magneto-photonic crystal waveguides," *Opt. Commun.*, vol. 199, pp. 389–397, Dec. 2001.
[9] H. Kato and M. Inoue, "Reflection-mode operation of 1-dimensional magnetophotonic crystals for use in film-based magneto-optical isolator devices," *J. Appl. Phys.*, vol. 91, pp. 7017–7019, May 2002.
[10] M. Koshiba and X. P. Zhuang, "An efficient finite-element analysis of magnetooptic channel waveguide," *J. Lightwave Technol.*, vol. 11, pp. 1453–1458, Sept. 1993.
[11] A. Erdmann, S. Shamonin, P. Hertel, and H. Dotsch, "Finite difference analysis of gyrotropic waveguides," *Opt. Commun.*, vol. 102, pp. 25–30, Sept. 1993.
[12] A. Erdmann and P. Hertel, "Beam-propagation in magnetooptic waveguides," *IEEE J. Quantum Electron.*, vol. 31, pp. 1510–1516, Aug. 1995.
[13] Y. Tsuji and M. Koshiba, "Finite element method using port truncation by perfectly matched layer boundary conditions for optical waveguide discontinuity problems," *J. Lightwave Technol.*, vol. 20, pp. 463–468, Mar. 2002.
[14] F. L. Teixeira and W. C. Chew, "General closed-form PML constitutive tensors to match arbitrary bianisotropic and dispersive linear media," *IEEE Microwave Guided Wave Lett.*, vol. 8, pp. 223–225, June 1998.
[15] M. Koshiba, Y. Tsuji, and S. Sasaki, "High-performance absorbing boundary conditions for photonic crystal waveguide simulations," *IEEE Microwave Wireless Components Lett.*, vol. 11, pp. 152–154, Apr. 2001.
[16] N. Bahlmann, M. Lohmeyer, H. Dötsch, and P. Hertel, "Integrated magneto-optic Mach–Zehnder interferometer isolator for TE modes," *Electron. Lett.*, vol. 34, pp. 2122–2123, May 1985.
[17] S. Boscolo, M. Midrio, and T. F. Krauss, "Y junctions in photonic crystal channel waveguide: High transmission and impedance matching," *Opt. Lett.*, vol. 27, pp. 1001–1003, June 2002.
[18] A. Chutinan, M. Okano, and S. Noda, "Wider bandwidth with high transmission through waveguide bends in two-dimensional photonic crystal slabs," *Appl. Phys. Lett.*, vol. 80, pp. 1698–1700, Mar. 2002.
[19] N. Bahlmann, M. Lohmeyer, O. Zhuromskyy, H. Dötsch, and P. Hertel, "Nonreciprocal coupled waveguides for integrated optical isolators and circulators for TM-modes," *Opt. Commun.*, vol. 161, pp. 330–337, Mar. 1999.

Naoya Kono was born in Kanagawa, Japan, on August 6, 1979. He received the B.S. degree in electronic engineering from Hokkaido University, Sapporo, Japan, in 2002. He is currently working toward the M.S. degree in electronics and information engineering at Hokkaido University.

Mr. Kono is a Student Member of the Institute of Electronics, Information and Communication Engineers (IEICE) of Japan.

Yasuhide Tsuji (M'97) was born in Takikawa, Japan, on December 31, 1967. He received the B.S., M.S., and Ph.D. degrees in electronic engineering from Hokkaido University, Sapporo, Japan, in 1991, 1993, and 1996, respectively.

In 1996, he joined the Department of Applied Electronic Engineering, Hokkaido Institute of Technology, Sapporo, Japan. Since 1997, he has been an Associate Professor of Hokkaido University. He has been engaged in research on wave electronics.

Dr. Tsuji is a Member of the Institute of Electronics, Information and Communication Engineers (IEICE) of Japan. He was awarded the Excellent Paper Awards from the IEICE in 1997 and 1999, and he was awarded the Young Scientist Award from the IEICE in 1999.